

New constraints on muon-neutrino to electron-neutrino transitions in MINOS

P. Adamson,⁸ C. Andreopoulos,²² D. J. Auty,²⁶ D. S. Ayres,¹ C. Backhouse,²⁰ G. Barr,²⁰ R. H. Bernstein,⁸ M. Betancourt,¹⁷ P. Bhattarai,¹⁸ M. Bishai,⁴ A. Blake,⁶ G. J. Bock,⁸ J. Boehm,⁹ D. J. Boehnlein,⁸ D. Bogert,⁸ C. Bower,¹² S. Budd,¹ S. Cavanaugh,⁹ D. Cherdack,²⁹ S. Childress,⁸ B. C. Choudhary,⁸ J. H. Cobb,²⁰ J. A. B. Coelho,⁷ S. J. Coleman,³¹ L. Corwin,¹² D. Cronin-Hennessy,¹⁷ I. Z. Danko,²¹ J. K. de Jong,^{20, 11} N. E. Devenish,²⁶ M. V. Diwan,⁴ M. Dorman,¹⁶ C. O. Escobar,⁷ J. J. Evans,¹⁶ E. Falk,²⁶ G. J. Feldman,⁹ M. V. Frohne,^{10, 3} H. R. Gallagher,²⁹ A. Godley,²⁴ M. C. Goodman,¹ P. Gouffon,²³ N. Graf,¹¹ R. Gran,¹⁸ E. W. Grashorn,¹⁷ K. Grzelak,³⁰ A. Habig,¹⁸ D. Harris,⁸ P. G. Harris,²⁶ J. Hartnell,^{26, 22} R. Hatcher,⁸ K. Heller,¹⁷ A. Himmel,⁵ A. Holin,¹⁶ X. Huang,¹ J. Hylen,⁸ J. Ilic,²² G. M. Irwin,²⁵ Z. Isvan,²¹ D. E. Jaffe,⁴ C. James,⁸ D. Jensen,⁸ T. Kafka,²⁹ S. M. S. Kasahara,¹⁷ G. Koizumi,⁸ S. Kopp,²⁸ M. Kordosky,³¹ Z. Krahn,¹⁷ A. Kreymer,⁸ K. Lang,²⁸ G. Lefeuvre,²⁶ J. Ling,²⁴ P. J. Litchfield,¹⁷ R. P. Litchfield,²⁰ L. Loiacono,²⁸ P. Lucas,⁸ J. Ma,²⁸ W. A. Mann,²⁹ M. L. Marshak,¹⁷ J. S. Marshall,⁶ N. Mayer,¹² A. M. McGowan,^{1, 17} R. Mehdiyev,²⁸ J. R. Meier,¹⁷ M. D. Messier,¹² D. G. Michael,^{5, *} W. H. Miller,¹⁷ S. R. Mishra,²⁴ J. Mitchell,⁶ C. D. Moore,⁸ J. Morfín,⁸ L. Mualem,⁵ S. Mufson,¹² J. Musser,¹² D. Naples,²¹ J. K. Nelson,³¹ H. B. Newman,⁵ R. J. Nichol,¹⁶ J. P. Ochoa-Ricoux,⁵ W. P. Oliver,²⁹ M. Orchanian,⁵ R. Ospanov,²⁸ J. Paley,^{1, 12} A. Para,⁸ R. B. Patterson,⁵ G. Pawloski,²⁵ G. F. Pearce,²² D. A. Petyt,¹⁷ R. Pittam,²⁰ R. K. Plunkett,⁸ R. A. Rameika,⁸ T. M. Raufer,²² B. Rebel,⁸ P. A. Rodrigues,²⁰ C. Rosenfeld,²⁴ H. A. Rubin,¹¹ V. A. Ryabov,¹⁴ M. C. Sanchez,^{13, 1, 9} J. Schneps,²⁹ P. Schreiner,³ P. Shanahan,⁸ W. Smart,⁸ C. Smith,¹⁶ A. Sousa,^{9, 20} M. Strait,¹⁷ S. Swain,²⁵ N. Tagg,^{19, 29} R. L. Talaga,¹ J. Thomas,¹⁶ M. A. Thomson,⁶ G. Tinti,²⁰ R. Toner,⁶ G. Tzanakos,² J. Urheim,¹² P. Vahle,³¹ B. Viren,⁴ A. Weber,²⁰ R. C. Webb,²⁷ C. White,¹¹ L. Whitehead,⁴ S. G. Wojcicki,²⁵ D. M. Wright,¹⁵ T. Yang,²⁵ K. Zhang,⁴ M. Zois,² and R. Zwaska⁸

(The MINOS Collaboration)

¹Argonne National Laboratory, Argonne, Illinois 60439, USA

²Department of Physics, University of Athens, GR-15771 Athens, Greece

³Physics Department, Benedictine University, Lisle, Illinois 60532, USA

⁴Brookhaven National Laboratory, Upton, New York 11973, USA

⁵Lauritsen Laboratory, California Institute of Technology, Pasadena, California 91125, USA

⁶Cavendish Laboratory, University of Cambridge, Madingley Road, Cambridge CB3 0HE, United Kingdom

⁷Universidade Estadual de Campinas, IFGW-UNICAMP, CP 6165, 13083-970, Campinas, SP, Brazil

⁸Fermi National Accelerator Laboratory, Batavia, Illinois 60510, USA

⁹Department of Physics, Harvard University, Cambridge, Massachusetts 02138, USA

¹⁰Holy Cross College, Notre Dame, Indiana 46556, USA

¹¹Physics Division, Illinois Institute of Technology, Chicago, Illinois 60616, USA

¹²Indiana University, Bloomington, Indiana 47405, USA

¹³Department of Physics and Astronomy, Iowa State University, Ames, Iowa 50011, USA

¹⁴Nuclear Physics Department, Lebedev Physical Institute, Leninsky Prospect 53, 119991 Moscow, Russia

¹⁵Lawrence Livermore National Laboratory, Livermore, California 94550, USA

¹⁶Department of Physics and Astronomy, University College London, Gower Street, London WC1E 6BT, United Kingdom

¹⁷University of Minnesota, Minneapolis, Minnesota 55455, USA

¹⁸Department of Physics, University of Minnesota – Duluth, Duluth, Minnesota 55812, USA

¹⁹Otterbein College, Westerville, Ohio 43081, USA

²⁰Subdepartment of Particle Physics, University of Oxford, Oxford OX1 3RH, United Kingdom

²¹Department of Physics and Astronomy, University of Pittsburgh, Pittsburgh, Pennsylvania 15260, USA

²²Rutherford Appleton Laboratory, Science and Technology Facilities Council, OX11 0QX, United Kingdom

²³Instituto de Física, Universidade de São Paulo, CP 66318, 05315-970, São Paulo, SP, Brazil

²⁴Department of Physics and Astronomy, University of South Carolina, Columbia, South Carolina 29208, USA

²⁵Department of Physics, Stanford University, Stanford, California 94305, USA

²⁶Department of Physics and Astronomy, University of Sussex, Falmer, Brighton BN1 9QH, United Kingdom

²⁷Physics Department, Texas A&M University, College Station, Texas 77843, USA

²⁸Department of Physics, University of Texas at Austin, 1 University Station C1600, Austin, Texas 78712, USA

²⁹Physics Department, Tufts University, Medford, Massachusetts 02155, USA

³⁰Department of Physics, University of Warsaw, Hoża 69, PL-00-681 Warsaw, Poland

³¹Department of Physics, College of William & Mary, Williamsburg, Virginia 23187, USA

(Dated: November 26, 2024)

This letter reports results from a search for $\nu_\mu \rightarrow \nu_e$ transitions by the MINOS experiment based on a 7×10^{20} protons-on-target exposure. Our observation of 54 candidate ν_e events in the Far

Detector with a background of $49.1 \pm 7.0(\text{stat.}) \pm 2.7(\text{syst.})$ events predicted by the measurements in the Near Detector requires $2 \sin^2(2\theta_{13}) \sin^2\theta_{23} < 0.12$ (0.20) at the 90% C.L. for the normal (inverted) mass hierarchy at $\delta_{CP} = 0$. The experiment sets the tightest limits to date on the value of θ_{13} for nearly all values of δ_{CP} for the normal neutrino mass hierarchy and maximal $\sin^2(2\theta_{23})$.

PACS numbers: 14.60.Pq, 14.60.Lm, 29.27.-a

Observations of neutrinos created in the Sun, in the Earth's atmosphere, at nuclear reactors, and by accelerators provide compelling evidence that neutrinos experience quantum mechanical mixing of their weak flavor states [1–7]. The resulting neutrino oscillations imply that neutrinos have mass and can be represented in either mass or flavor bases, related by the 3×3 PMNS neutrino mixing matrix [8]. This matrix parameterizes the mixing amplitude using three angles (θ_{12} , θ_{23} , and θ_{13}), two Majorana phases [9], and a phase (δ_{CP}) that could give rise to charge-parity (CP) violation in the lepton sector. The oscillation probability depends on the differences in the squared masses of the neutrino states and the ratio (L/E) of the distance the neutrino travels to the energy of the neutrino.

In MINOS, the larger mass splitting dominates, and oscillations are manifested primarily as the energy dependent disappearance of muon-neutrinos. MINOS has set the most precise measurement of the mass splitting $|\Delta m^2| = (2.43 \pm 0.13) \times 10^{-3} \text{ eV}^2$ [7, 10] and requires $\sin^2(2\theta_{23}) > 0.9$ at the 90% confidence level (C.L.). At this mass splitting scale, it is expected that the ν_μ are changing predominantly into ν_τ ; however the subdominant $\nu_\mu \rightarrow \nu_e$ transition mode is not excluded [1]. Such transitions would indicate a non-zero value of θ_{13} , the unknown angle of the PMNS matrix and could open the possibility of observing CP violation in the lepton sector. In this letter, we report new results from the search for $\nu_\mu \rightarrow \nu_e$ transitions.

The most stringent constraint on θ_{13} , from the CHOOZ reactor experiment [11], implies $\sin^2(2\theta_{13}) < 0.15$ at the 90% C.L. for the value of $|\Delta m^2|$ measured by MINOS. However, a recent global analysis of oscillation measurements hints at a non-zero value for θ_{13} [12]. The CHOOZ limit is based on a measurement of the probability for electron-antineutrino disappearance. MINOS measures the probability of electron-neutrino appearance, which additionally depends on $\sin^2\theta_{23}$, δ_{CP} , and the sign of Δm^2 . MINOS is the first experiment to probe $\sin^2(2\theta_{13})$ with sensitivity beyond the CHOOZ limit. An initial measurement with 3.14×10^{20} protons-on-target (POT) yielded 35 observed ν_e -like events with an expected background of $27 \pm 5(\text{stat.}) \pm 2(\text{syst.})$ events [13]. This 1.5σ excess of events is consistent with a value of $\sin^2(2\theta_{13})$ near the CHOOZ limit. The present analysis is based on an integrated exposure of 7.01×10^{20} protons-on-target and includes the data set from the previous analysis.

In MINOS, interactions of neutrinos produced in the Fermilab NuMI beam line [14] are observed in two detec-

tors: a Near Detector (ND) with a 29 t fiducial mass 1.04 km from the production target and a Far Detector (FD) with a 4 kt fiducial mass 735 km from the target. Both detectors are magnetized tracking calorimeters, composed of planes of 2.54 cm thick steel and 1.0 cm thick scintillator (1.4 radiation lengths per plane). The scintillator planes are segmented into 4.1 cm wide strips (1.1 Molière radii) [15]. The high statistics data set collected at the ND establishes the properties of the mostly ν_μ beam before oscillations. The signature of $\nu_\mu \rightarrow \nu_e$ oscillations is an excess of ν_e interactions in the FD relative to the expected background based on the ND observation.

Neutrino flavor can be identified in charged current (CC) interactions by the event topology produced by the associated charged lepton. Muons deposit energy consistent with a minimum ionizing particle that can be tracked through successive detector planes (a track). Electrons, on the other hand, deposit energy in a relatively narrow and short region (an electromagnetic shower). Additional detector activity can be produced by the breakup of the recoil nucleus and other particles produced in the interaction.

In this analysis, the dominant backgrounds to ν_e -CC events are neutral current (NC) interactions and ν_μ -CC interactions with low energy muons. These interactions can produce signatures that are similar to those of ν_e -CC events, especially when the hadronic system includes a π^0 . An irreducible background arises from the 1.3% $\nu_e + \bar{\nu}_e$ component of the beam. This beam ν_e background results primarily from decays of muons produced in pion and kaon decays. Their rate below 8 GeV is well constrained by the measured ν_μ energy spectrum [7, 16]. Smaller background components come from cosmogenic sources and CC interactions of ν_τ coming from $\nu_\mu \rightarrow \nu_\tau$ oscillations.

Selection criteria are applied to events to isolate ν_e -CC interactions and suppress backgrounds. Cosmogenic backgrounds in this analysis are reduced to less than 0.3 events (90% C.L.) in the FD by applying directional requirements and requiring the events to be in time with the accelerator pulse. Selected events must have reconstructed energy between 1 and 8 GeV, a reconstructed shower, and at least 5 contiguous planes, each with energy depositions above half the energy deposited by a minimum ionizing particle. Events with long tracks are rejected. Further enrichment is achieved using an artificial neural network (ANN) with 11 input variables characterizing the longitudinal and transverse energy depo-

sition in the calorimeter [17]. The variables used in the ANN are identical to those used in [13], but the network was re-optimized over a sample of simulated events generated with a refined detector response model, improved event reconstruction, and better modeling of hadron scattering within the iron nucleus. Maximum sensitivity is achieved by selecting events with the neural network output above 0.7. Background rejection is improved by a factor of 1.2 over that reported in [13] for a similar signal efficiency.

The number of expected background events is determined from ND data. The extrapolation to the FD of each of the primary background components, ν_μ -CC, NC, and beam ν_e -CC, has a different dependence on oscillation probability and beam geometry and is treated separately. Individual background components are determined using three beam configurations, each with different relative background compositions. The first configuration is the standard one used for the appearance search. The hadron production target is located close to the first focusing horn, producing a neutrino beam peaked at 3 GeV. In the second configuration, the target is moved upstream from the horns causing higher energy hadrons to be focused and yielding a neutrino spectrum peaked at 9 GeV. In a third configuration the current in the focusing horns is turned off so no hadrons are focused. Consequently, the low-energy peak of the neutrino energy distribution disappears, and the selected event sample is dominated by NC events from higher energy neutrino interactions.

Data obtained in the above configurations and the simulated ratios of rates for each configuration are used to extract the three individual background spectra. The beam line, detector, and particle propagation simulation is based on GEANT3 [18] and the hadron production yields from the target are based on FLUKA [19]. Neutrino interactions and further re-interactions of the resulting hadrons within the nucleus are simulated using NEUGEN3 [20]. The predicted neutrino energy spectrum is adjusted to agree with the ND ν_μ -CC data [16].

Data were collected during three run periods, each with somewhat different beam conditions. Most notably, during the third run period, the decay pipe was filled with helium at 0.9 atm for safety reasons. The background decomposition is performed as a function of neutrino energy and is done separately for each run period to account for the different beam conditions, a small, gradual target degradation, and detector aging. Figure 1 shows the energy spectrum measured in the ND for events passing the selection criteria and the extracted NC, ν_μ -CC, and beam ν_e -CC components. The ND background is $(64\pm 5)\%$ NC, $(23\pm 5)\%$ ν_μ -CC and $(13\pm 3)\%$ beam ν_e -CC events. The errors on the components are derived primarily from the data and are correlated due to the constraint that the background must add up to the observed ND event rate. This constraint also leads to a much reduced error on

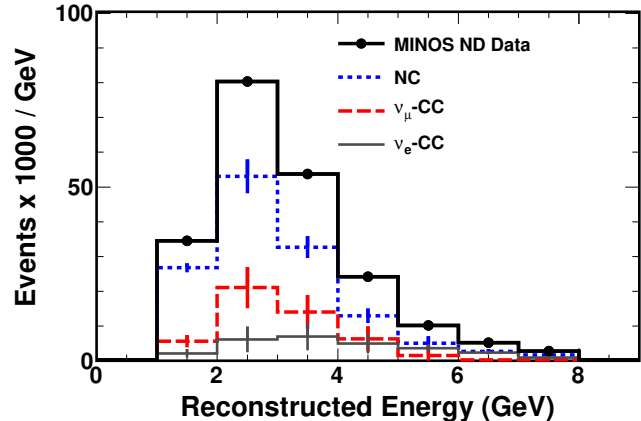


FIG. 1: Reconstructed Near Detector energy spectra of the ν_e -CC selected events (bold solid). Also shown is the decomposition of this spectrum into neutral current (dotted), ν_μ charged current (dashed), and beam ν_e -CC (light solid) components determined using the multiple beam configuration method. The sum of the three background components is constrained to agree with the data. Uncertainties on the data are statistical and are not visible on this scale; uncertainties on the components are systematic.

the FD prediction. A second decomposition technique was applied to verify the background components. This method uses ν_μ -CC events with the muon track removed. The remnant hits are then processed through the standard analysis [13, 21]. This second method yields consistent ND background components.

After decomposition of the ND data from each run period into separate background components, each spectrum is multiplied by the ratio of FD to ND event rates in reconstructed energy bins based on the simulation for that component, providing a prediction of the FD spectrum in the absence of ν_e appearance. Neutrino oscillations are included when predicting the FD event rate. The predictions are summed to give 49.1 expected background events, of which 35.8 are NC, 6.3 ν_μ -CC, 5.0 beam ν_e and 2.0 ν_τ [22].

The efficiency for selecting ν_e -CC events is estimated using remnants from muon-removed ν_μ -CC events with a simulated electron replacing the muon. The embedded electron has the same momentum and direction as the removed muon. Test beam measurements [23] demonstrate that single electrons are well modeled in the MINOS detectors, and the selection efficiency of electrons agrees with the simulation to within 1.6%. With this method, we find our efficiency for selecting ν_e -CC events to be $(41.6\pm 1.0)\%$.

Systematic uncertainties are evaluated by generating Monte Carlo (MC) samples in which systematic effects are varied over their expected range of uncertainty and quantifying the change in the number of predicted back-

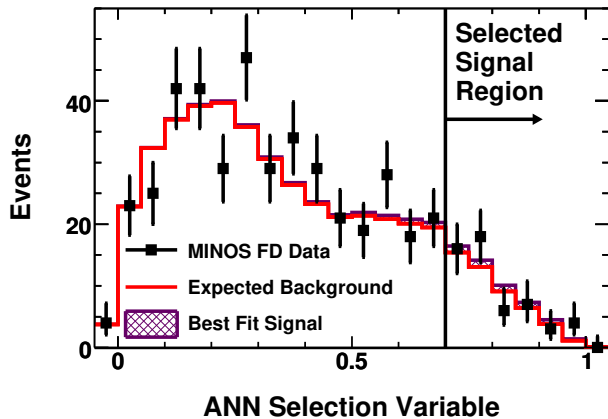


FIG. 2: Distribution of the ANN selection variable for pre-selected events in the Far Detector. Black points show data with statistical error bars. The non-shaded histogram shows the expected background. The shaded region shows the additional ν_e charged current events allowed from the best fit to the oscillation hypothesis as described in the text.

ground events in the FD. Most of the dominant uncertainties arise from Far/Near differences. The principal systematic effects, listed in Table I, include (a) uncertainties in energy scale, (b) uncertainty in Near to Far relative event rate, and (c) uncertainties in the nuclear hadronization and intranuclear scattering models. Other systematic error sources (d) including uncertainties in cross section models, beam flux, and the details of the detector simulation each contribute to the systematic error at lower levels. While uncertainties in the composition and kinematic distribution of the particles that emerge from the nucleus can be large, these and other uncertainties associated with neutrino interaction physics mostly cancel when comparing the ND and FD data. The use of the same materials and detector segmentation in the ND and FD is critical in achieving this error cancellation. The individual systematic errors on the expected background are combined in quadrature with the uncertainty from the decomposition of the background and a systematic error on the ν_τ background to give an overall systematic uncertainty of 5.6% on the expected number of background events in the FD.

The expected number of background events and its uncertainty, along with all the analysis procedures are established before examining the full FD data set. Additionally, before counting events in the signal region of $\text{ANN} > 0.7$, two FD data samples are examined to check the expected event rate and the background rejection in the FD. To verify the expected event rate, the full decomposition and extrapolation method is applied to events well below the signal region ($\text{ANN} < 0.5$), giving a prediction of 313.6 events. We observe 327 events, consistent with the prediction to within 1σ . Background rejection

Uncertainty source	Uncertainty on background events
Far/Near ratio:	4.5%
(a) Energy Scale	2.8%
(b) Relative Event Rate	2.4%
(c) Hadronic Model	2.5%
(d) All Other Combined	0.7%
Near Detector Decomposition	2.8%
ν_τ background	1.7%
Total Systematic Uncertainty	5.6%
Expected Statistical Uncertainty	14.3%

TABLE I: Systematic uncertainty in the total number of background events in the Far Detector.

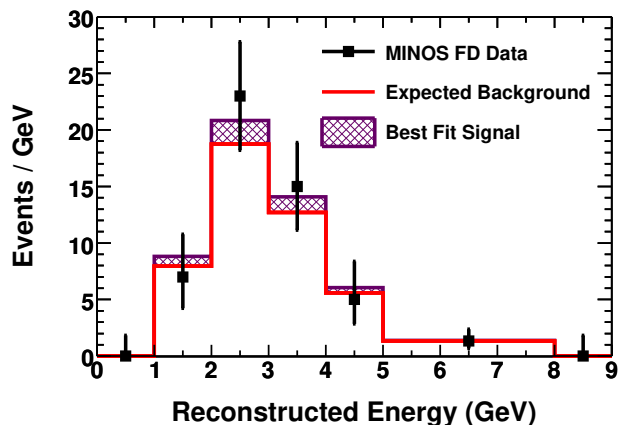


FIG. 3: Reconstructed energy spectrum of the events in the Far Detector which pass all ν_e charged current selection criteria, with the exception of the energy cut. Black points show data with statistical error bars. The non-shaded histogram shows the expected background. The shaded region shows the additional ν_e charged current events allowed by the best fit to the oscillation hypothesis.

is verified by examining muon-removed ν_μ -CC events. In the FD (92.8 ± 0.9 (stat.)%) of muon removed events are rejected, in agreement with (93.58 ± 0.05 (stat.)%) predicted from the ND data.

Figure 2 shows the number of selected candidate events in the FD as a function of the ANN selection variable. The energy spectrum for the events in the signal region is shown in Figure 3. We observe 54 events in the signal region with an expected background of 49.1 ± 7.0 (stat.) ± 2.7 (syst.), a 0.7σ excess over the expected background. Similar results were produced by a cross check analysis that used a different neural network based on an alternate event reconstruction algorithm [24]. Taking into account the improved background rejection in the current analysis, this result is consistent with the earlier report, based on a smaller data sample. From that sample we now select 28 events with an expected background of 22.5 ± 4.7 (stat.) ± 1.1 (syst.) events.

Figure 4 shows the values of $2\sin^2(2\theta_{13})\sin^2\theta_{23}$ and

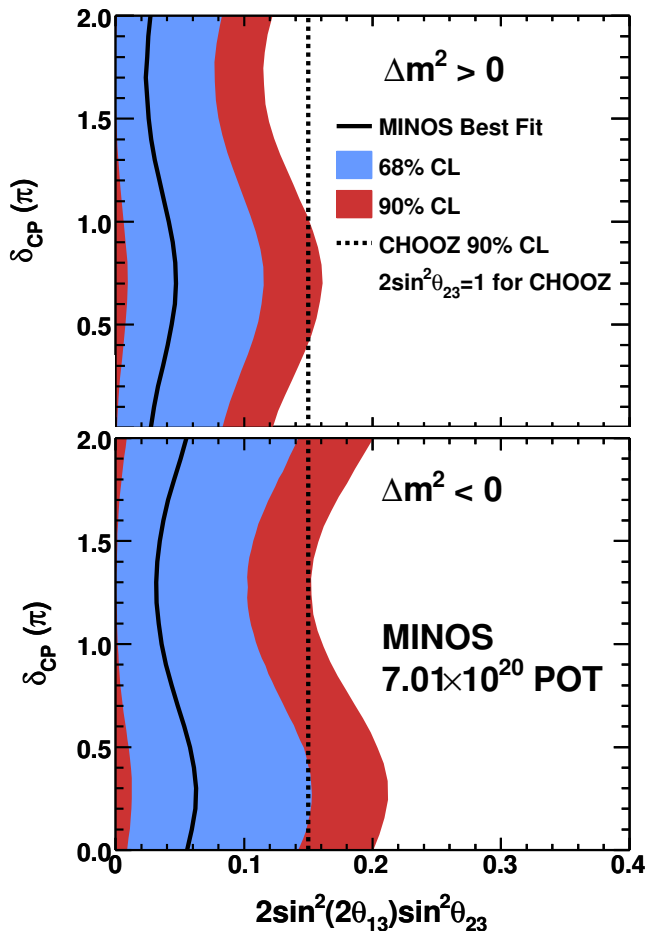


FIG. 4: Values of $2 \sin^2(2\theta_{13}) \sin^2\theta_{23}$ and δ_{CP} that produce a number of candidate events in the Far Detector consistent with the observation for the normal hierarchy (top) and inverted hierarchy (bottom). Black lines show those values that best represent our data. Red (blue) regions show the 90% (68%) C.L. intervals. The CHOOZ limit is drawn for $\Delta m_{32}^2 = 2.43 \times 10^{-3} \text{eV}^2$, $\sin^2(2\theta_{23}) = 1.0$

δ_{CP} that give a number of events consistent with our observation. The oscillation probability is computed using a full 3-flavor neutrino mixing framework with matter effects [25, 26], which includes a dependence on the neutrino mass hierarchy. Statistical and systematic uncertainties are included when constructing the confidence intervals via the Feldman-Cousins approach [27]. The variations of the values of $|\Delta m_{32}^2|$, Δm_{21}^2 , $\sin^2\theta_{23}$, and $\sin^2(2\theta_{12})$ within their experimental errors [1, 5–7] are included in the computation of the contours.

In conclusion, we report improved constraints on $2 \sin^2(2\theta_{13}) \sin^2\theta_{23}$ from the search for ν_e appearance by the MINOS experiment. The 54 events selected in the Far Detector are 0.7σ higher than the expected background of $49.1 \pm 7.0(\text{stat.}) \pm 2.7(\text{syst.})$. Interpreted as an upper limit on the probability of $\nu_\mu \rightarrow \nu_e$ oscillations,

our data require $2 \sin^2(2\theta_{13}) \sin^2\theta_{23} < 0.12$ (0.20) at the 90% C.L. at $\delta_{CP} = 0$ for the normal (inverted) hierarchy. This measurement represents the best constraint on the value of θ_{13} for nearly all values of δ_{CP} assuming the normal mass hierarchy and maximal $\sin^2(2\theta_{23})$.

This work was supported by the US DOE; the UK STFC; the US NSF; the State and University of Minnesota; the University of Athens, Greece; and Brazil's FAPESP, CNPq, and CAPES. We are grateful to the Minnesota DNR, the crew of the Soudan Underground Laboratory, and the staff of Fermilab for their contributions to this effort.

* Deceased.

- [1] Y. Ashie *et al.*, Phys. Rev. Lett. **93**, 101801 (2004); Phys. Rev. D **71**, 112005 (2005).
- [2] W.W.M. Allison *et al.*, Phys. Rev. D **72**, 052005 (2005).
- [3] M. Ambrosio *et al.*, Eur. Phys. J. C **36**, 323 (2004).
- [4] M.H. Ahn *et al.*, Phys. Rev. D **74**, 072003 (2006).
- [5] B. Aharmim *et al.*, Phys. Rev. C **72**, 055502 (2005).
- [6] T. Araki *et al.*, Phys. Rev. Lett. **94**, 081801 (2005).
- [7] P. Adamson *et al.*, Phys. Rev. Lett. **101**, 131802 (2008).
- [8] B. Pontecorvo, JETP **34**, 172 (1958); V.N. Gribov and B. Pontecorvo, Phys. Lett. B **28**, 493 (1969); Z. Maki, M. Nakagawa, and S. Sakata, Prog. Theor. Phys. **28**, 870 (1962).
- [9] Oscillation experiments are not sensitive to the Majorana phases.
- [10] The experiment measures an unresolved mixture of $|\Delta m_{31}^2|$ and $|\Delta m_{32}^2|$ which we refer to as $|\Delta m^2|$ for brevity. For further discussion see G. Fogli *et al.*, Prog. Part. Nucl. Phys. **57**, 742 (2006).
- [11] M. Apollonio *et al.*, Eur. Phys. J. C **27**, 331 (2003).
- [12] G.L. Fogli *et al.*, Phys. Rev. Lett. **101**, 141801 (2008).
- [13] P. Adamson *et al.*, Phys. Rev. Lett. **103**, 261802 (2009).
- [14] S. Kopp, Proc. 2005 IEEE Part. Accel. Conf., May 2005, Fermilab-Conf-05-093-AD and arXiv:physics/0508001.
- [15] D.G. Michael *et al.*, Nucl. Inst. & Meth. A **596**, 190 (2008).
- [16] P. Adamson *et al.*, Phys. Rev. D **77**, 072002 (2008).
- [17] T. Yang, Ph.D. Thesis, Stanford University (2009).
- [18] R. Brun *et al.*, CERN Program Library W5013 (1984).
- [19] A. Fasso *et al.*, CERN-2005-10 (2005).
- [20] S. Dytman, H. Gallagher, and M. Kordosky, arXiv:0806.2119 (2008).
- [21] A. Holin, Ph.D. Thesis, UCL (2010).
- [22] For $\Delta m_{32}^2 = 2.43 \times 10^{-3} \text{eV}^2$, $\sin^2(2\theta_{23}) = 1.0$, and $\sin^2(2\theta_{13}) = 0$.
- [23] P. Adamson *et al.*, Nucl. Inst. & Meth. A **556**, 119 (2006); A. Cabrera *et al.*, Nucl. Inst. & Meth. A **609**, 106 (2009).
- [24] S. Cavanaugh, Ph.D. Thesis, Harvard University (2010).
- [25] E.K. Akhmedov *et al.*, J. High En. Phys. **0404**, 078 (2004).
- [26] J. Boehm, Ph.D. Thesis, Harvard University (2009).
- [27] G.J. Feldman and R.D. Cousins, Phys. Rev. D **57**, 3873 (1998).